GLIA

WILEY

RESEARCH ARTICLE

SorCS2 facilitates release of endostatin from astrocytes and controls post-stroke angiogenesis

Anna R. Malik[1,2] ![ORCID] | Janet Lips[3,4,5] | Malgorzata Gorniak-Walas[1] |
Diede W. M. Broekaart[6] | Antonino Asaro[1] | Melanie T. C. Kuffner[3,4] |
Christian J. Hoffmann[3,4] | Majed Kikhia[3,4,7] | Monika Dopatka[3,4] |
Philipp Boehm-Sturm[3,4,8] | Susanne Mueller[3,4,8] | Ulrich Dirnagl[3,4,5,7,9] |
Eleonora Aronica[6,10] | Christoph Harms[3,4,5,7] | Thomas E. Willnow[1]

[1]Max-Delbrueck-Center for Molecular Medicine, Berlin, Germany

[2]Nencki Institute of Experimental Biology, Polish Academy of Sciences, Warsaw, Poland

[3]Department of Experimental Neurology, Charité—Universitätsmedizin Berlin and Berlin Institute of Health, Neurocure Cluster of Excellence, Berlin, Germany

[4]Charité—Universitätsmedizin Berlin, Center for Stroke Research Berlin, Berlin, Germany

[5]Berlin Institute of Health, QUEST Centre for Transforming Biomedical Research, Berlin, Germany

[6]Amsterdam UMC, University of Amsterdam, Department of (Neuro) Pathology, Amsterdam Neuroscience, Amsterdam, the Netherlands

[7]Charité—Universitätsmedizin Berlin, Einstein Center for Neurosciences Berlin, Berlin, Germany

[8]Charité—Universitätsmedizin Berlin, Charité Core Facility 7T Experimental MRIs, Berlin, Germany

[9]German Centre for Neurodegenerative Diseases, Berlin, Germany

[10]Stichting Epilepsie Instellingen Nederland (SEIN), Heemstede, The Netherlands

Correspondence
Anna R. Malik, Nencki Institute of Experimental Biology, Pasteura-Str. 3, 02-093 Warsaw, Poland.
Email: a.malik@nencki.edu.pl

Thomas E. Willnow, Max-Delbrueck-Center for Molecular Medicine, Robert-Roessle-Str. 10, 13125 Berlin, Germany.
Email: willnow@mdc-berlin.de

Funding information
Berlin Institute of Health, Grant/Award Number: TRG7; Deutsche Forschungsgemeinschaft, Grant/Award Numbers: EXC-2049 - 390688087, HA5741/5-1, HO5177/3-1, GSC 203; Fundacja na rzecz Nauki Polskiej, Grant/Award Number: 5CEF/18-00; German Federal Ministry of Education and Research, Grant/Award Numbers: 01EO1301, 01EW1811; H2020 European Research Council, Grant/Award Number: 335692

Abstract

SorCS2 is an intracellular sorting receptor of the VPS10P domain receptor gene family recently implicated in oxidative stress response. Here, we interrogated the relevance of stress-related activities of SorCS2 in the brain by exploring its role in ischemic stroke in mouse models and in patients. Although primarily seen in neurons in the healthy brain, expression of SorCS2 was massively induced in astrocytes surrounding the ischemic core in mice following stroke. Post-stroke induction was likely a result of increased levels of transforming growth factor $\beta1$ in damaged brain tissue, inducing *Sorcs2* gene transcription in astrocytes but not neurons. Induced astrocytic expression of SorCS2 was also seen in stroke patients, substantiating the clinical relevance of this observation. In astrocytes in vitro and in the mouse brain in vivo, SorCS2 specifically controlled release of endostatin, a factor linked to post-stroke angiogenesis. The ability of astrocytes to release endostatin acutely after stroke was lost in mice deficient for SorCS2, resulting in a blunted endostatin response which coincided with impaired vascularization of the ischemic brain. Our findings identified activated astrocytes as a source for endostatin in modulation of post-stroke

angiogenesis, and the importance of the sorting receptor SorCS2 in this brain stress response.

KEYWORDS

cytokine, glial scar, ischemia, protein sorting, VPS10P domain receptors

1 | INTRODUCTION

SorCS2 is a member of the VPS10P domain receptors gene family, a unique class of sorting receptors expressed in neurons of the mammalian nervous system (Willnow, Petersen, & Nykjaer, 2008). VPS10P domain receptors are best recognized for their ability to shuttle target proteins between intracellular compartments and the neuronal cell surface. By doing so, they regulate the surface exposure of neuronal receptors or activity-dependent secretion of signaling molecules, as shown for neurotrophin receptors or brain-derived neurotrophic factor, respectively (Z.-Y. Chen et al., 2005; Vaegter et al., 2011). The relevance of neuronal protein sorting by VPS10P domain receptors is underscored by their causal involvement in psychiatric and neurodegenerative diseases, including Huntington's disease, Alzheimer's disease, and frontotemporal dementia (Reitz, 2015; Willnow et al., 2008).

Recently, we documented that SorCS2 is unique among the various VPS10P domain receptors as its expression is up-regulated in response to oxidative stress and epilepsy in neurons (Malik et al., 2019). Under these conditions, SorCS2 promotes cell surface sorting of the neuronal amino acid transporter EAAT3, facilitating EAAT3-mediated uptake of cysteine for production of the reactive oxygen species scavenger glutathione (Malik et al., 2019). Ultimately, induced expression of SorCS2 enables neurons to cope with oxidative stress and protects them from seizure-induced cell death.

To explore a global role for SorCS2 as a stress-induced protein in multiple brain injuries, we here assessed its significance in stroke, a pathological condition linked to severe oxidative stress. Surprisingly, while up-regulation of SorCS2 expression was observed in an experimental mouse model of stroke, this induction was specific to astrocytes, a cell type that normally does not express this receptor. In activated astrocytes, SorCS2 controlled secretion of endostatin and promoted post-stroke angiogenesis. Our findings corroborated a role for SorCS2 as a stress-induced factor and uncovered its cell type-specific actions in protection from brain injuries, such as ischemic stroke.

2 | MATERIALS AND METHODS

2.1 | Mouse models

Mice with a targeted disruption of murine *Sorcs2* (KO) have been described (Glerup et al., 2014). KO males and wild-type littermate controls (WT) used for in vivo studies were 8–14 weeks of age, generated by heterozygous breedings on an inbred C57BL/6N background. Animals were kept under 12 hr/12 hr light/dark cycle with free access to food and water. Newborn mice for astrocytic and neuronal cultures were obtained by homozygous breeding of the respective WT or KO strains. Animal experimentation was performed following approval by local committees of the State of Berlin (X9012/12, X9007/17, G 0157/17).

2.2 | Human tissue samples

Brain tissue samples used in this study for immunostainings were obtained from the archives of the department of Neuropathology of the Amsterdam UMC (University of Amsterdam, the Netherlands). Three acute stroke cases (injury-death interval <2 weeks) and four autopsy controls without any history of neurologic diseases were included. Supporting Information Table S1 summarizes the clinical characteristics of patients and controls. The age and gender did not differ between stroke patients and autopsy controls ($p > .05$, Mann Whitney U test). Material for primary astrocyte cultures was collected after a written informed consent for the use of the material for research purposes had been obtained by the Bloemenhove clinic from all donors. All human specimens were obtained and used in accordance with the Declaration of Helsinki and the Amsterdam UMC Research Code provided by the Medical Ethics Committee of the AMC. Local ethical committees of the participating centers gave permission to undertake the study.

2.3 | Middle cerebral artery occlusion

Filamentous occlusion of the middle cerebral artery was performed as described (Dirnagl & Members of the MCAO-SOP Group, 2012). Mice were anaesthetized using 2.5% (vol/vol) isoflurane for induction and 1.5% (vol/vol) isoflurane for maintaining anesthesia in a mixture with 25% O_2 and 75% N_2O. Cerebral ischemia was induced by introducing a 8–0 silicon-rubber coated suture (Doccol Corp., Sharon, MA) into the left internal carotid artery and by advancing it to the anterior cerebral artery, thereby occluding the middle cerebral artery. The filament was withdrawn after an occlusion time of 45 min. Body temperature was maintained at $37.0 \pm 0.5°C$ throughout the experiment using a feed-back controlled heating pad and a rectal probe (Fine Science Tools GmbH, Heidelberg). During middle cerebral artery occlusion (MCAo) and for at least 2 hr after reperfusion, animals were allowed to recover in a heated cage (Peco Services, Cumbria, UK).

Mice were randomized and blinded for concealment of genetic group allocation and the order of surgery. In the short-term studies

(1 and 3 days), no mortality was observed and no mice were excluded from analysis. In the long-term study (21 days) 4 WT (21%) and 4 KO (20%) died within 1 week after MCAo and mice with no stroke (technical failure; 2 WT and 2 KO) or stroke volume approximately <3 mm^3 (3 WT and 3 KO) were excluded from analysis.

2.4 | Brain vasculature labeling

Mice were anesthetized with Ketamine/Xylazine and a solution of DyLight488-labeled *Lycopersicon esculentum* lectin (#DL-1174 Vectorlab) was injected intravenously (1 mg/ml; 4 μl per gram bodyweight). After 180 s, mice were transcardially perfused with 4% paraformaldehyde (PFA)/phosphate-buffered saline (PBS). Brains were isolated and incubated in 4% PFA in PBS (overnight) and in 30% sucrose/PBS (72 hr), and frozen in −40°C isopentane prior to sectioning. A total of 3 WT mice and 1 KO mouse were excluded from the vessels analysis because of technical failures of lectin staining (heart arrest during injection or bad circulation).

2.5 | Cell culture experiments

Cultures enriched in astrocytes were prepared from newborn mice according to published protocols (Parnis et al., 2013). In brief, blood vessels and meninges were removed from cortical tissue which was next trypsinized and dissociated in presence of DNAse. Cells were plated on poly-L-lysine-coated flasks and cultured in Dulbecco's Modified Eagle's Medium (DMEM) with 10% FBS and penicillin/streptomycin. After 2 days, cells were washed to remove cellular debris. After 7 days in vitro, cultures were shaken extensively to remove microglia and the astrocytes were plated for experiments.

Cells were treated with 10 ng/ml transforming growth factor β (TGF-β1; R&D Biosystems, 7666-MB) in serum-free DMEM for 3, 6, 24, or 48 hr. Control cells were incubated in DMEM for 24 hr. For cytokines measurements, astrocytes were stimulated with 100 nM Phorbol 12-myristate 13-acetate (PMA) and 2.5 μM ionomycin for 3 hr or left untreated (control). For endostatin measurements, astrocytes were washed and incubated in serum-free DMEM for 24 hr.

Neuronal cultures were prepared from hippocampi and cortices of newborn mice as described earlier (Malik et al., 2019). In brief, cultures were prepared using enzymatic digestion with papain and plated at the density of 83,000 cells/cm^2. After 10 days in culture, the cells were treated with 10 ng/ml TGF-β1 for 6, 24 or 48 hr or left untreated.

Human primary fetal astrocyte-enriched cultures were obtained from human fetal brain tissue (14–19 weeks of gestation) obtained from medically-induced abortions. Cells isolation was performed as described (Aronica, Gorter, Rozemuller, Yankaya, & Troost, 2005). Briefly, the tissue was digested with trypsin, mechanically disrupted, and the cell suspension was plated in DMEM/Ham's F10 (1:1) medium supplemented with penicillin/streptomycin and 10% fetal calf serum. Cultures reached confluence after 2–3 weeks. Secondary astrocyte cultures for experimental manipulation were used at passage 2–5.

Cells plated on poly-L-lysine-coated plates were stimulated with human recombinant TGF-β1 (Peprotech, 10 ng/ml) for 24 hr.

2.6 | ELISA measurements

Sample preparation is described in Supporting Information. Following enzyme-linked immunosorbent assay (ELISA) kits were used: TGF-β1 (Abcam, ab119557), GFAP (Millipore, NS830), endostatin (Boster, EK1376), U-Plex Biomarker Group 1 assay (Meso Scale Diagnostics, K15083K). For technical reasons, not all the samples were included in GFAP and TGF-β1 ELISA measurements. Brain and blood plasma samples used for endostatin measurements were selected based on the results of tissue sections stainings and GFAP ELISA measurements to include mice with similar lesion area and localization and comparable GFAP levels.

2.7 | Protein array

Proteome Profiler Mouse Angiogenesis Array Kit (R&D Systems, ARY015) was used according to manufacturer's instructions. Used tissue samples were selected based on the results of tissue sections stainings and GFAP ELISA measurements to include mice with similar lesion area and localization and comparable GFAP levels. Tissue lysates were prepared as for ELISA, diluted in Array Buffer 6 and the total amount of 350 μg protein was loaded on the membrane. Signal intensities were measured with use of LI-COR Imaging System and quantified with Image Studio Lite software. In one experiment, four samples (WT ipsi, WT contra, KO ipsi, KO contra; ipsi and contra samples from the same mouse brain) were processed and analyzed in parallel. Signal intensities were normalized to the mean value obtained for a given protein in contralateral samples (WT and KO) in the same experiment. In total, the experiment was repeated 3 times on different pairs (WT and KO) of mice and the results were combined.

2.8 | Immunostaining

Following antibodies were used: anti-SorCS2 (R&D Systems, AF4237, 1:100, for mouse tissue and cells; rabbit anti-SorCS2, Lifespan Biosciences, LS-C501334, 1:450, for human tissue), Cy3-labeled anti-GFAP (Sigma, C9205, 1:1,000, for mouse tissue and cells), anti-GFAP (monoclonal mouse, Sigma, 1:4,000, for human tissue), biotinylated anti-NeuN (Millipore, MAB377B, 1:100, for murine tissue), mouse anti-NeuN (Millipore, MAB377 (clone A60), 1:2,000, for human tissue). Details on samples preparation and staining protocols are given in Supporting Information.

2.9 | Western blot

Tissue and cell lysates were analyzed by western blot using the following antibodies: anti-SorCS2 (R&D Systems, AF4237, 1:1,000),

anti-p-ERK (Cell Signaling, 4370, 1:2,000), anti-actin (Abcam, ab8227, 1:2,000), anti-GFAP (Millipore, MAB360, 1:1,000). Signal was registered with digital LI-COR imaging system and quantified using the Image Studio Lite software.

2.10 | Quantitative RT-PCR

RNA was extracted using TRIzol reagent and purified with RNeasy Mini Kit (QIAGEN). Reversely transcribed cDNA was subjected to quantitative real-time polymerase chain reaction (qRT-PCR) analysis. For murine samples, following Taqman Gene Expression Assays were used: Actb (actin, Mm02619580), GAPDH (Mm99999915), Col18a1 (collagen XVIII, Mm00487131), and SORCS2 (Mm00473050). Col18a1 and SorCS2 transcript levels were shown relative to Actb or GAPDH as specified in the respective figure legends. For human samples, SYBR Green method was used with the following PCR primers: *SORCS2* (forward: GTTTGTCATCGGGCTCTTCG, reverse: GTCCTGCCTGGCCGTTTC) and *EF1a* (forward: ATCCACCTTTGGGTCGCTTT, reverse: CCGCAACTGT CTGTCTCATATCAC). *SORCS2* transcript levels were given relative to EF1α as described (Ramakers, Ruijter, Deprez, & Moorman, 2003; Ruijter et al., 2009).

2.11 | Image analysis

Stroke lesion size was analyzed with use of ImageJ software. Lesions and whole brain sections were marked manually based on the images of NeuN, GFAP and DAPI stainings and their areas were measured. For 1 KO mouse, measuring lesion size was not possible due to technical problems with sectioning. Areas covered by blood vessels were analyzed automatically with use of Cell Profiler software. Vessels length was analyzed manually with use of ImageJ software with NeuronJ plugin. For comparison between the two hemispheres of individual mouse brains, data were normalized to the mean value obtained for the contralateral side. For comparison between the two genotypes, data were normalized to the mean value obtained for WT mice analyzed in the same set.

2.12 | Statistical analysis

For in vivo experiments, an indicated number n is the number of mice per group, and for astrocytic and neuronal culture experiments n is the number of independent preparations (biological replicates) used. The study was powered according to the ARRIVE guidelines to detect differences in cytokine levels using two-way analysis of variance (ANOVA) for side and genotype interactions with α error probe of 0.05 and Power of 0.8 and 0.7 effect size based on F tests with critical $F = 3.5$ for a minimum number of $n = 6$ per sample size (G*Power 3.1.9.2). Statistical analyses were performed using GraphPad Prism software. For comparison between two experimental groups, a two-tailed unpaired t test was used with the exception of direct comparison of TGF-β1 levels in the two hemispheres of the same mouse brain where paired t test was used. For data with three or more groups and one independent variable, one-way ANOVA with Dunnett's multiple comparisons test was used. For data with two independent variables, two-way ANOVA with Tukey's multiple comparisons test was applied. For ELISA and western blot quantifications, outlier analysis was performed using Grubb's and ROUT tests and individual datapoints were excluded accordingly. The details of statistical analysis are specified in the figure legends.

3 | RESULTS

3.1 | SorCS2 is induced in astrocytes surrounding the ischemic core

To query the significance of SorCS2 for ischemic stroke, we subjected mice either wild-type (WT) or genetically deficient for *Sorcs2* (KO) to 45 min of transient MCAo, an experimental model commonly used in mice (Dirnagl & Members of the MCAO-SOP Group, 2012). In WT brains 3 days after MCAo, immunostaining for neuronal (NeuN) and astrocytic (GFAP) markers revealed severe neuronal cell loss and astrogliosis in the ipsilateral hemisphere (Figure 1a). SorCS2 expression in these brains was massively induced in reactive astrocytes within the glial scar surrounding the ischemic core (region 1, Figure 1b,c) and to a lesser extent also in other regions adjacent to the lesion (regions 2 and 4, Figure 1b,c). Little to no SorCS2 expression was seen in astrocytes in the contralateral hemisphere (regions 3 and 5, Figure 1b,c). Induced expression in activated astrocytes was surprising as SorCS2 expression in the normal murine brain is predominantly seen in neuronal cell types (Glerup et al., 2014), particularly in neurons of the hippocampal CA2 region, in pyramidal neurons of the cerebral cortex, and in striatal neurons (Supporting Information Figure S1). Post-stroke induction of SorCS2 expression was restricted to astrocytes as no overt increase in neuronal SorCS2 immunoreactivity was seen 1 (Supporting Information Figure S2) or 3 days after ischemic stroke (Figure 1b,c and Supporting Information Figure S3). Similar to the situation in mouse models, SorCS2 expression in the healthy human brain was primarily visible in neurons and only occasionally in astrocytes (Supporting Information Figure S4). However, SorCS2 expression was up-regulated in astrocytes following ischemia in stroke patients, corroborating the clinical relevance of our observations (Figure 1d).

Ischemic stroke triggers release of multiple cytokines and growth factors that promote tissue regeneration. Of note, increased levels of TGF-β were reported in the plasma of stroke patients (Yan, Greer, & McCombe, 2012) and its expression was induced in the murine brain following ischemia (Zhang et al., 2018). TGF-β has been implicated in processes of post-stroke recovery, including glial scaring and angiogenesis (Meng et al., 2016; Pardali, Goumans, & ten Dijke, 2010; Zhu et al., 2017). In line with these findings, we detected increased levels of TGF-β1 in the ipsilateral hemispheres of the WT brains 3 days after MCAo (Figure 2a). Application of TGF-β1 induced levels of SorCS2 transcript (Figure 2b) and protein (Figure 2c,d) in primary murine astrocytes.
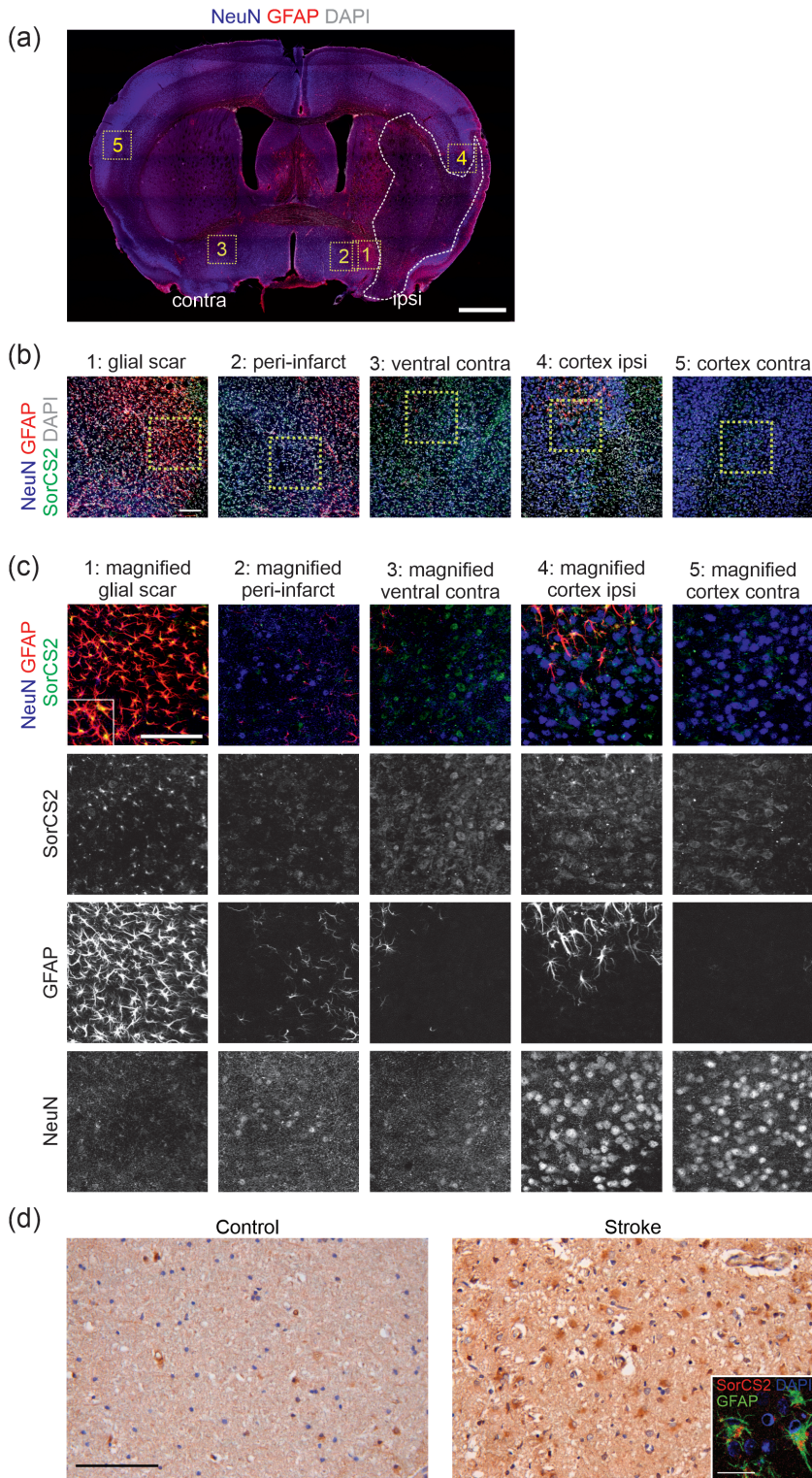
FIGURE 1 SorCS2 expression is induced in astrocytes after ischemic stroke. (a) Coronal brain section of a wild-type mouse 3 days after 45 min MCAo. Sections were immunostained for GFAP (red; astrocytes) and NeuN (blue; neurons), and counterstained with DAPI (grayscale). Scale bar, 1 mm. Ipsilateral (ipsi) and contralateral (contra) hemispheres are indicated. The ischemic core is indicated by white dashed line. Numbered yellow dashed boxes highlight regions shown in (b). (b) Representative images of brain sections stained for GFAP (red; astrocytes), NeuN (blue; neurons), SorCS2 (green), and counterstained with DAPI (grayscale) as marked in (a). Yellow dashed boxes indicate regions shown as higher magnification images in (c). Maximum intensity projections of confocal z-sections are shown. Scale bar, 50 μm. (c) Higher magnification of regions indicated in (b). The upper row of panels shows merged images for GFAP (red, astrocytes), NeuN (blue, neurons), and SorCS2 (green) immunosignals. Panels below show the separated channels in grayscale. Robust SorCS2 expression in GFAP-positive cells in the glial scar region is visible. By contrast, no increase in neuronal SorCS2 signal intensities is seen in any of the analyzed regions of the ipsilateral as compared to the contralateral side. The inset in the image of the glial scar region shows a higher magnification of SorCS2-positive astrocytes. Maximum intensity projections of confocal z-sections are shown. Scale bar, 50 μm. (d) SorCS2 immunostaining (brown) in the human control brain and in the brain of a patient after stroke. The inset in the right panel shows cells immunofluorescently stained for SorCS2 (red) and astrocyte marker GFAP (green) in post-stroke brain tissue. Scale bars: overview, 100 μm; inset, 25 μm

Similarly, SorCS2 mRNA levels were also increased in cultured human fetal astrocytes by TGF-β1 treatment (Figure 2e). By contrast, induction was not observed in primary neurons treated with TGF-β1 (Figure 2f), providing a possible molecular explanation for the astrocyte-specific induction of SorCS2 expression following ischemic stroke.
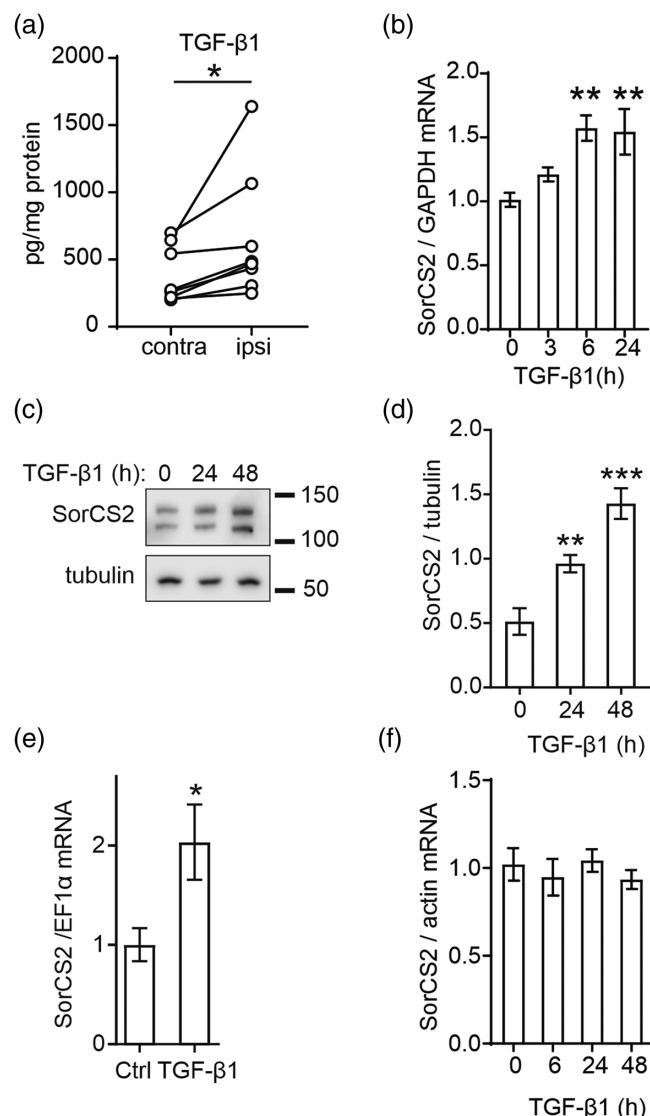
3.2 | SorCS2-deficient mice show normal post-stroke astrocyte activation and cytokines levels

To elaborate on the role of SorCS2 in activated astrocytes, we performed a comparative analysis of stroke-driven astrogliosis in WT

animals and in mice lacking this receptor (KO). Three days after MCAo, the size of the ischemic lesion was similar in both genotypes (Figure 3a,b). Also, the extent of astrocyte activation in the ipsilateral hemisphere was comparable as shown by immunodetection of GFAP on histological sections (Figure 3a) and in brain lysates (Figure 3c,d).

Activated astrocytes drive inflammatory responses through release of cytokines. To investigate the consequence of SorCS2 deficiency on this response, we performed cytokine profiling of ipsi- and contralateral hemispheres of WT and KO mice 3 days after MCAo. Among the tested cytokines, IL-1β, IL-5, IL-10, IL-13, IL-16, IL-17A, IL-17C, IL-21, IL-22, IL-23, and IFNγ showed no differences in levels between ipsi- and contralateral hemispheres (Supporting Information - Figure S5). GM-CSF, TNFα, KC/GRO, IL-2, MCP-1, MIP-1α, MIP-2, IP-10, EPO, MIP-1β, MIP-3α, and IL-12p70 were up-, while VEGF-A was down-regulated in ipsilateral as compared to contralateral hemispheres (Figure 3e and Supporting Information Figure S5). However, this response was seen in WT and KO mice to a similar extent.

3.3 | SorCS2-deficient mice fail to induce endostatin expression after stroke

To identify factors secreted from astrocytes in a SorCS2-dependent manner, we assayed the levels of proteins relevant for post-injury regeneration using protein arrays. Three days after MCAo, levels of coagulation factor III and FGF1 did not differ remarkably between ipsi- and contralateral hemispheres (Figure 4a and Supporting Information Figure S6). Osteopontin, CXCL4, CCN3, serpin E1, and IGFBP2 increased in the ipsilateral hemisphere regardless of *Sorcs2* genotype (Figure 4a and Supporting Information Figure S6). However, increases in levels of IGFBP3 and endostatin in the ipsilateral hemisphere were seen in WT but not KO brains, suggesting SorCS2 dependency (Figure 4a–c).

The association of plasma IGFBP3 levels with *SORCS2* in humans had been reported (Kaplan et al., 2011), validating our screening approach for identifying SorCS2 targets in the ischemic brain. Here, we focused on endostatin, a potent anti-angiogenic factor produced from collagen XVIII by proteolysis (Sasaki et al., 1998). Prior studies had implicated endostatin in post-stroke recovery (Gertz et al., 2006; Navarro-Sobrino et al., 2011). We confirmed the impact of SorCS2 on endostatin levels by showing that endostatin levels increased twofold in the ipsilateral as compared to the contralateral hemisphere of WT brains at 3 days after MCAo. This effect was lost in KO mice (Figure 4d). The rise in endostatin levels in the ipsilateral WT hemisphere correlated with the lesion size (Figure 4e) and was specific to

FIGURE 2 TGF-β1 increases after ischemic stroke and induces SorCS2 expression in primary astrocytes. (a) TGF-β1 levels in contralateral (contra) and ipsilateral (ipsi) hemispheres of WT brains at 3 days after MCAo were determined by ELISA and normalized to total protein content. Values obtained for individual mice are presented as connected dots. *n* = 7 mice. *, *p* < .05 in paired *t* test. (b) Transcript levels of SorCS2 in primary murine astrocytes treated with TGF-β1 (10 ng/ml) for the indicated times were measured by qRT-PCR and given relative to transcript levels of GAPDH. Fold change relative to untreated cells (time = 0, set to 1) is shown. Mean ± *SEM* is indicated. *n* = 10 independent astrocytic preparations. **, *p* < .01 when compared to time = 0 by one-way ANOVA with Dunett's multiple comparisons test. (c) Western blot analysis of SorCS2 levels in primary murine astrocytes treated with TGF-β1 (10 ng/ml) for the indicated times in hours (h). Detection of tubulin serves as a loading control. (d) Quantification of SorCS2 levels normalized to tubulin signal as depicted in (c). *n* = 7 independent astrocytic preparations. **, *p* < .01, ***, *p* < .001 when compared to time = 0 by one-way ANOVA with Dunett's multiple comparisons test. (e) Transcript levels of SorCS2 in cultured human fetal astrocytes treated with TGF-β1 (10 ng/ml) for 24 hr as measured by qRT-PCR and given relative to transcript levels of EF1α. Fold change relative to untreated cells (Ctrl, set to 1) is shown. Mean ± *SEM* is indicated. *n* = 6 samples derived from three donors (two replicates per donor). *, *p* < .05 by unpaired *t* test. (f) Transcript levels of SorCS2 in primary murine neurons treated with TGF-β1 (10 ng/ml) for the indicated times as measured by qRT-PCR and given relative to transcript levels of actin. Fold change relative to untreated cells (time = 0, set to 1) is shown. Mean ± *SEM* is indicated. *n* = 6 independent neuronal preparations
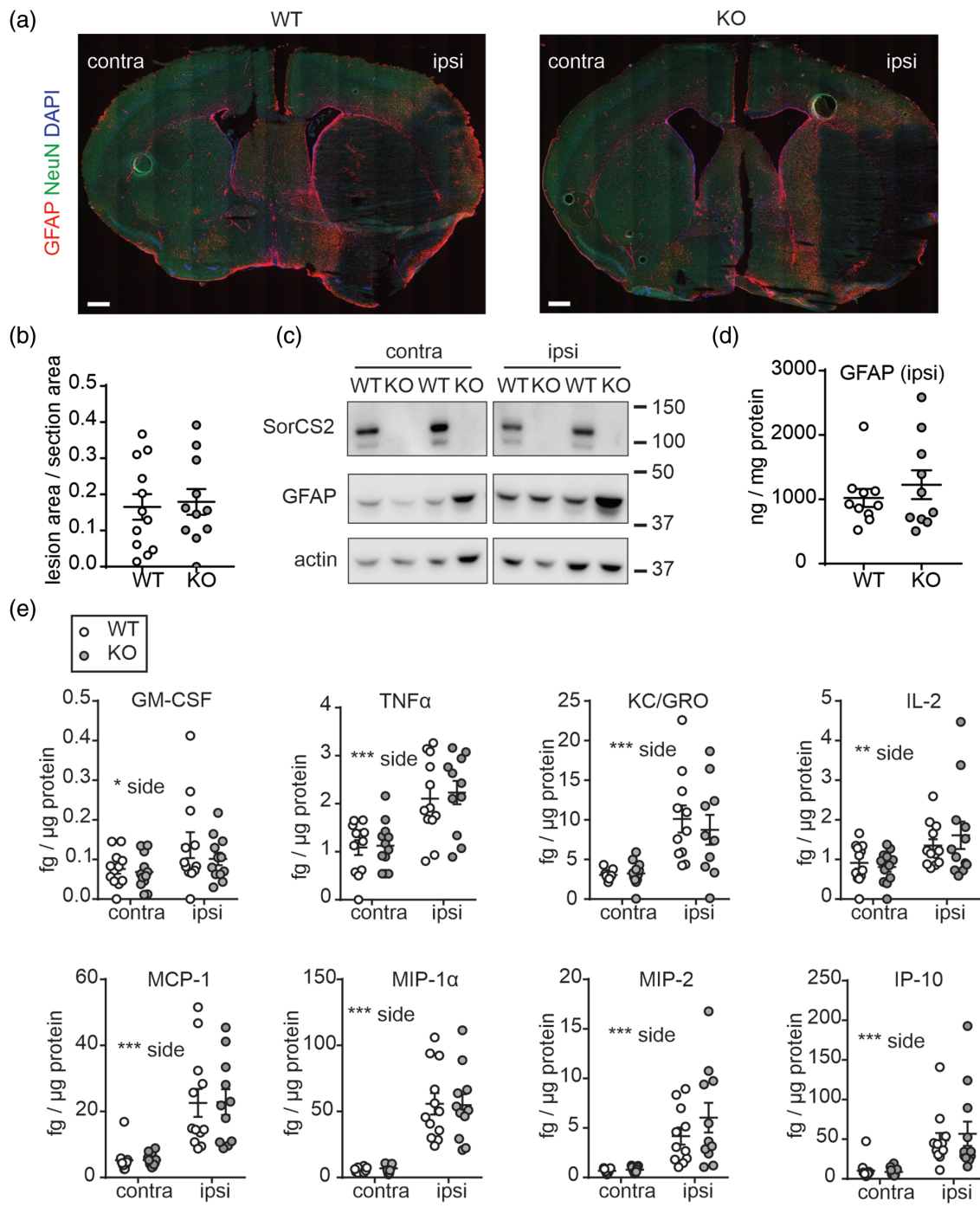
FIGURE 3 Normal glia activation and neuroinflammation in the post-stroke brain of KO mice. (a) Representative images of coronal brain sections of WT and KO mice at 3 days after MCAo. Sections were immunostained for GFAP (red) and NeuN (green), and counterstained with DAPI (blue). The extent of activation of GFAP-labeled astrocytes and the loss of NeuN-positive neurons in the ipsilateral (ipsi) as compared to the contralateral (contra) side is similar in both genotypes. Scale bars, 500 μm. (b) Quantification of the stroke lesion areas on histological sections of WT and KO brains as exemplified in (a). n = 11–12 mice per genotype. Mean ± *SEM* is given. (c) Western blot analysis of GFAP levels in lysates prepared from ipsilateral (ipsi) and contralateral (contra) hemispheres of 2 WT and 2 KO mice 3 days after MCAo. Detection of SorCS2 and actin was used as controls. (d) Levels of GFAP in ipsilateral hemispheres of WT and KO brains 3 days after MCAo were determined by ELISA. GFAP levels were normalized to total protein content. Mean ± *SEM* is indicated. n = 10 mice per genotype. (e) Results of ELISA measurements of cytokines levels in tissue lysates from ipsilateral (ipsi) and contralateral (contra) hemispheres of WT and KO brains 3 days after MCAo. Cytokines levels were normalized to total protein content. n = 12 mice per genotype. Mean ± *SEM* is indicated. *, $p < .05$; **, $p < .01$; ***, $p < .001$ by two-way ANOVA. See Supporting Information Figure S5 for the measurements of additional cytokines in these tissue extracts. GM-CSF, granulocyte-macrophage colony-stimulating factor; TNFα, tumor necrosis factor alpha; KC/GRO, growth-regulated alpha protein; IL-2, interleukin 2; MCP-1, monocyte chemoattractant protein 1; MIP-1α, macrophage inflammatory protein 1-alpha; MIP-2, macrophage inflammatory protein 2; IP-10, interferon gamma-induced protein 10
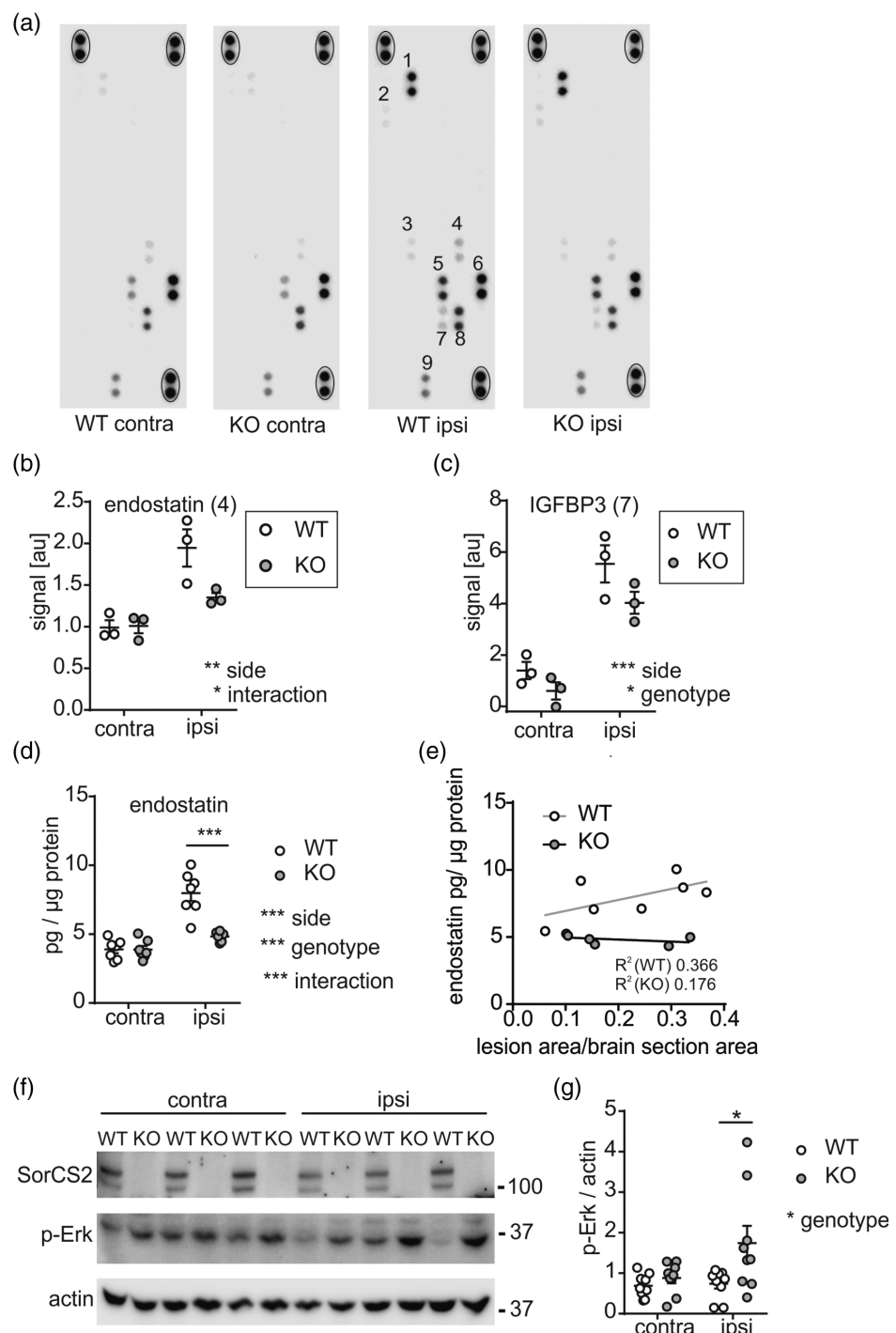
FIGURE 4 Endostatin levels are up-regulated after MCAo in a SorCS2-dependent manner. (a) Representative results of a proteome profiling array performed on ipsilateral (ipsi) and contralateral (contra) brain samples from WT and KO mice 3 days after MCAo. Each protein is detected in duplicate dots. Encircled dots represent positive controls. Selected protein spots are labeled by numbers. 1—osteopontin, 2—serpin E1, 3—CXCL4 (C-X-C motif chemokine 4), 4—endostatin, 5—IGFBP2 (insulin-like growth factor-binding protein 2), 6—coagulation factor III, 7—IGFBP3 (insulin-like growth factor-binding protein 3), 8—FGF1 (fibroblast growth factor 1), 9—CCN3 (CCN family member 3). (b and c) Quantification of signal intensities for endostatin (b; spot 4 in panel (a)) and IGFBP3 (c; spot 7 in panel (a)) obtained in proteome profiling array as depicted in (a). $n = 3$ mice per genotype. Mean ± SEM is indicated. *, $p < .05$; **, $p < .01$; ***, $p < .001$ by two-way ANOVA. See Supporting Information Figure S6 for quantifications of signal intensities for additional proteins. (d) Endostatin levels in tissue samples from ipsilateral and contralateral hemispheres of WT and KO mice 3 days after MCAo. Endostatin levels were measured by ELISA and normalized to total protein content in the tissue samples. $n = 6$–7 mice per genotype. Mean ± SEM is indicated. ***, $p < .001$ by two-way ANOVA with Tukey's multiple comparisons test. (e) Endostatin levels in the ipsilateral hemispheres in WT and KO mice 3 days after MCAo plotted against the respective stroke lesion sizes. R^2 indicates the goodness of fit for the linear regression. $n = 6$–7 mice per genotype. (f) Representative western blot analysis of p-Erk levels in ipsilateral and contralateral hemispheres of WT and KO mice 3 days after MCAo. Detection of SorCS2 and actin is shown as controls. (g) Quantification of p-Erk levels normalized to actin signal intensities in ipsilateral and contralateral hemispheres of WT and KO brains as depicted in (f). $n = 9$ mice per genotype. Mean ± SEM is indicated. *, $p < .05$ by two-way ANOVA with Tukey's multiple comparisons test
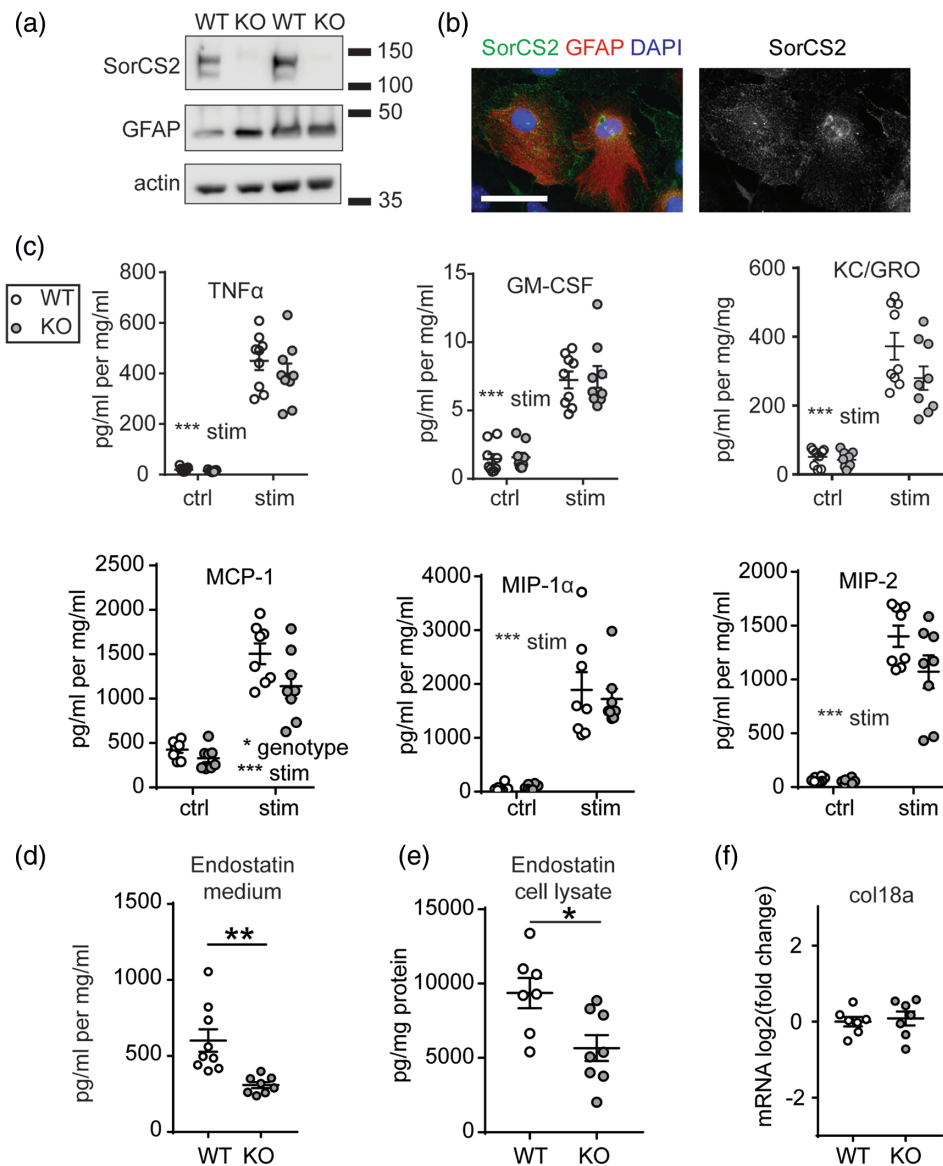
FIGURE 5 SorCS2 controls endostatin release from primary astrocytes. (a) SorCS2 expression in cultured primary astrocytes from WT and KO mice as determined by western blotting. Each lane represents an independent astrocyte preparation. Detection of GFAP and actin was used as loading control. (b) Representative image of immunostaining for SorCS2 (green) in primary cultured astrocytes from WT mice. Cells were co-stained for GFAP (red) and counterstained with DAPI (blue). Combined signals (left) and SorCS2 staining in grayscale (right) are shown. Scale bar, 50 μm. (c) Cytokines levels as determined by ELISA in cell culture medium from primary WT and KO astrocytes either untreated (ctrl) or treated with PMA/ionomycin (stim). Cytokines levels were normalized to the protein content in the respective cell lysates. $n = 9$ independent astrocyte preparations per group. Mean ± *SEM* is indicated. *, $p < .05$; ***, $p < .001$ by two-way ANOVA. See Supporting Information Figure S8 for the measurement of additional cytokines in these samples. TNFα, tumor necrosis factor alpha; GM-CSF, granulocyte-macrophage colony-stimulating factor; KC/GRO, growth-regulated alpha protein; MCP-1, monocyte chemoattractant protein 1; MIP-1α, macrophage inflammatory protein 1-alpha; MIP-2, macrophage inflammatory protein 2. (d) Endostatin levels in cell medium from primary WT or KO astrocyte cultures conditioned for 24 hr. Endostatin levels were quantified by ELISA and normalized to the protein content in the respective cell lysates. $n = 9$ independent astrocyte preparations per genotype. Mean ± *SEM* is indicated. **, $p < .01$ by unpaired t test. (e) Endostatin levels in cell lysates from primary WT or KO astrocyte cultures were measured by ELISA and normalized to the protein content. $n = 8$ independent astrocyte preparations per genotype. Mean ± *SEM* is indicated. *, $p < .05$ by unpaired t test. (f) Transcript levels of the endostatin precursor collagen 18a in astrocyte cell lysates as measured by qRT-PCR and given relative to transcript levels of actin. Log_2(fold change) relative to WT is shown. Mean ± *SEM* is indicated. $n = 7$ independent astrocyte preparations per genotype

the brain, as no changes in plasma endostatin levels were seen in affected WT animals (Supporting Information Figure S7). Endostatin acts on target cells through interference with signaling pathways, including the mitogen-activated protein kinase pathway (N. Chen, Gao, Yuan, & Zhao, 2016; Sudhakar et al., 2003). Consistent with this fact, increased endostatin levels in the ipsilateral hemispheres of WTs

corresponded with lower p-Erk levels as compared with the ipsilateral hemispheres of KOs (Figure 4f,g).

To further corroborate the role of astrocytic SorCS2 in endostatin release, we used primary astroglial cultures that express SorCS2 when kept in serum-supplemented medium (Figure 5a,b). Substantiating our findings from the MCAo experiments, SorCS2-deficient astrocytes were able to normally secret multiple cytokines after PMA/ionomycin

stimulation when compared with WT cells (Figure 5c and Supporting Information Figure S8). However, their ability to release endostatin was significantly impaired (Figure 5d). Endostatin levels were also lower in cell lysates from KO as compared with WT astrocytes (Figure 5e). In conclusion, astrocytes were able to produce and release endostatin in a process that depended on SorCS2. Transcript levels of the endostatin precursor collagen XVIII were not different between
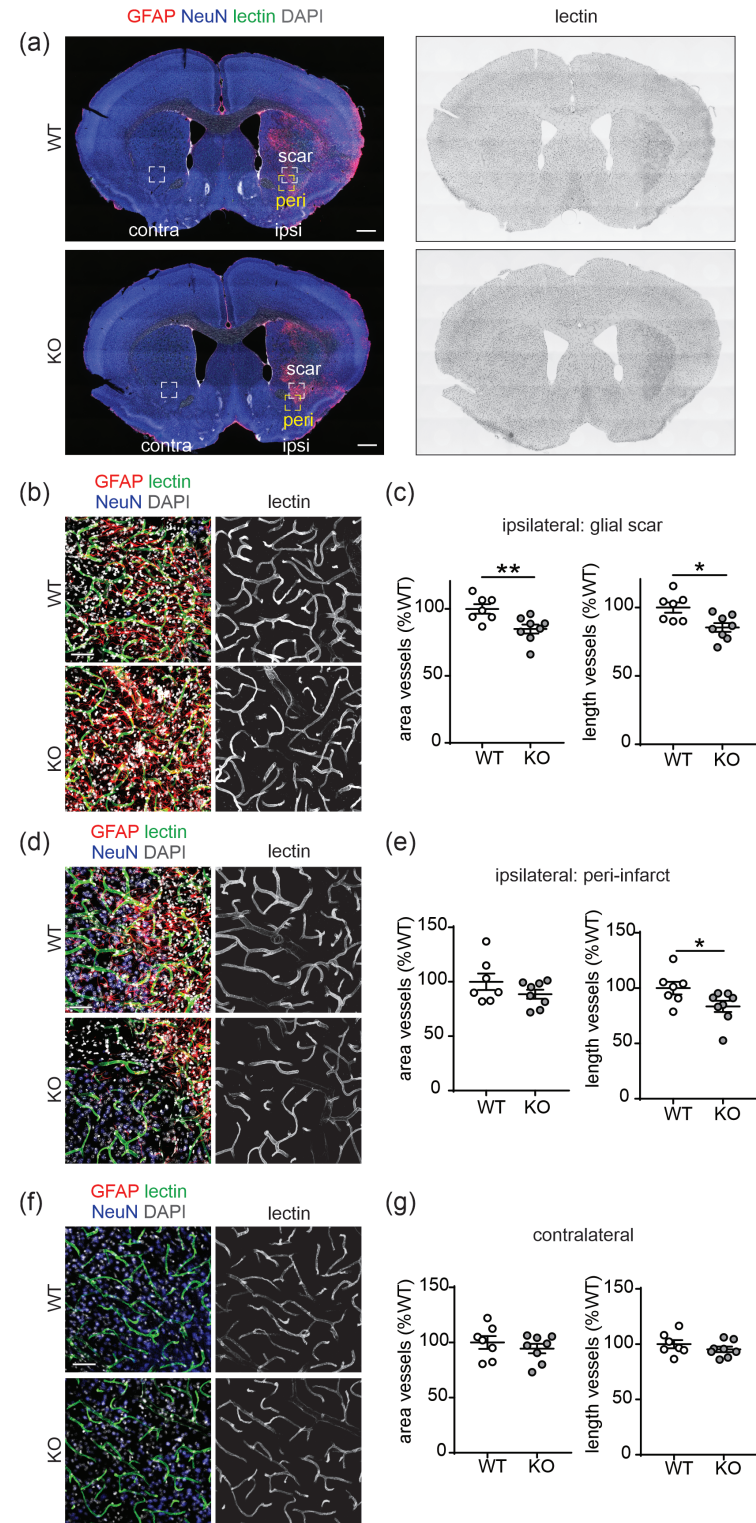

FIGURE 6 SorCS2 deficiency impairs post-stroke angiogenesis. (a) Representative images of coronal brain sections of WT and KO mice 21 days after MCAo. Mice were injected with DyLight488-lectin (green) to visualize blood vessels. In addition, the sections were immunostained for GFAP (red; astrocytes) and NeuN (blue; neurons) and counterstained with DAPI (grayscale). Left panels show combined signals for all channels, while right panels show DyLight488-lectin signal in grayscale. Dashed lines indicate regions analyzed in (b–g); scar, glial scar region; peri, peri-infarct region. Scale bars, 500 μm. (b) Representative images of glial scar regions in ipsilateral hemispheres of WT and KO mice brains as indicated in (a). Maximum intensity projections of confocal z-sections are shown. Scale bar, 50 μm. (c) Quantification of brain areas covered by vessels and vessels length in the glial scar region of WT and KO brains 21 days after MCAo (as depicted in (b)). n = 7–8 mice per genotype. Mean ± SEM is indicated. *, p < .05; **, p < .01 by unpaired t test. (d) Representative images of peri-infarct regions in ipsilateral hemispheres of WT and KO mice brains as indicated in (a). Maximum intensity projections of confocal z-sections are shown. Scale bar, 50 μm. (e) Quantification of brain areas covered by vessels and vessels length in the peri-infarct regions of WT and KO brains 21 days after MCAo (as depicted in (d)). n = 7–8 mice per genotype. Mean ± SEM is indicated. *, p < .05 by unpaired t test. (f) Representative images of contralateral hemispheres of WT and KO mouse brains as indicated in (a). Maximum intensity projections of confocal z-sections are shown. Scale bar, 50 μm. (g) Quantification of brain areas covered by vessels and vessels length in contralateral hemispheres of WT and KO brains 21 days after MCAo (as depicted in (f)). n = 7–8 mice per genotype. Mean ± SEM is indicated

the genotypes, suggesting a post-transcriptional mechanism of SorCS2-controlled endostatin release from astrocytes (Figure 5f).

3.4 | SorCS2-dependent release of endostatin promotes post-stroke angiogenesis

Next, we explored the consequence of SorCS2-induced production of endostatin for post-stroke angiogenesis. To do so, we injected WT and KO mice at 21 days after MCAo with DyLight 488-labeled lectin to mark functional vessels (Figure 6a). This time point is commonly used to study revascularization of the post-stroke murine brain (J.-Y. Chen et al., 2017; Rust et al., 2019).

Ischemic stroke triggers angiogenesis in areas adjacent to the lesion (Hayashi, Noshita, Sugawara, & Chan, 2003; Krupinski, Kaluza, Kumar, Kumar, & Wang, 1994). In line with this concept, blood vessels length was increased in the glial scar region in the WT brains, as compared with the contralateral side (Supporting Information Figure S9). However, this response was not seen in KO brains (Supporting Information Figure S9). More detailed analysis revealed that the length of the vessels but also the overall area covered by vessels were significantly reduced in the glial scar area in KO mice as compared with WTs (Figure 6b,c). A statistically significant decrease in vessel length in KO as compared with WT brains was also seen in the peri-infarct area (Figure 6d,e). No differences in vessel length and coverage were seen comparing the contralateral hemispheres of WT and KO mice (Figure 6f,g), strongly arguing that SorCS2 deficiency does not influence blood vessels formation during ontogeny but only during post-stroke angiogenesis. In summary, we uncovered a link between SorCS2 activity, endostatin release, and angiogenesis in the post-ischemic brain.

4 | DISCUSSION

Astrocytes are crucial players in stroke pathogenesis (reviewed in Pekny et al., 2016). We now show that activated astrocytes surrounding the ischemic core induce expression of SorCS2, a remarkable finding considering that expression of this sorting receptor in the brain has so far only been reported in neurons. Possibly, induction of SorCS2 expression in astrocytes is a pathophysiological response to increased levels of TGF-β1 in the post-stroke brain, which induces receptor gene transcription in astrocytes but not in neurons. While activated astrocytes define both infarct size and post-lesion recovery in stroke, SorCS2 deficiency had no impact on the ischemic lesion size. Instead, SorCS2 appears to have a specialized role in promoting post-stroke tissue regeneration, in particular in angiogenesis. While we cannot rule out with certainty that neuronal activities of SorCS2 may contribute to post-stroke phenotypes, all of our findings strongly argue that its role in recovery after ischemic insult depends on astrocytic expression of the receptor.

Given the prominent role of astrocytes in the inflammatory brain response, an impact of SorCS2 on their ability to release cytokines

may have been anticipated. Such a function had been shown for the related VPS10P domain receptor sortilin in T-cells (Herda et al., 2012). However, cytokine profiling in mouse brains and in activated primary astrocytes failed to document any SorCS2-dependent alterations. Rather, our studies uncovered the ability of SorCS2 to facilitate production and/or release of endostatin from this cell type. Endostatin is cleaved from its precursor collagen XVIII by various proteases, including cathepsins and metalloproteinases (Felbor et al., 2000; Ferreras, Felbor, Lenhard, Olsen, & Delaissé, 2000; Ma et al., 2007). To date, it is not clear which protease plays the major role in generating endostatin in vivo and whether processing takes place intracellularly or in the extracellular space. Thus, we can only speculate by what mechanism SorCS2 promotes endostatin production. Other VPS10P domain receptors sort cathepsins (Canuel, Korkidakis, Konnyu, & Morales, 2008), and SorCS2 may have a similar function in astrocytes to control proteolysis of collagen XVIII by these proteases.

Because of the decisive role of endostatin in formation of new blood vessels, it is tempting to speculate that impaired post-stroke angiogenesis in SorCS2-deficient mice may be causally linked to altered endostatin release from astrocytes in these mice. Endostatin blocks extracellular matrix-dependent motility and morphogenesis in numerous cell types (Kuo et al., 2001). Its anti-proliferative and anti-migratory effects on endothelial cells profoundly inhibit angiogenesis in tumor models (O'Reilly et al., 1997). Long-term treatment with endostatin abolishes the pro-angiogenic effects of physical activity in post-stroke mice (Gertz et al., 2006). In humans, high plasma levels of endostatin after stroke predict a worse long-term functional outcome (Navarro-Sobrino et al., 2011). We now show an increase in endogenous endostatin levels in the ischemic brain as a physiological response acutely after stroke (Figure 4). A similar surge in endostatin levels after stroke has been observed by others in rats (Hou et al., 2010) and rabbits (Tian, Chen, Cui, Xu, & Zhou, 2007). Increased post-stroke release of endostatin seems counterintuitive given the need of the injured brain to grow new vessels. However, previous studies indicated that the levels of both pro- and anti-angiogenic factors are induced after stroke and that these factors show dynamically regulated expression profiles (Hayashi et al., 2003). For example, levels of the angiogenesis inhibitor thrombospondin-1 transiently decrease 1 day after stroke to increase at 3 days post-ischemia. These findings highlight important temporal aspects of orchestrating post-stroke angiogenesis, and suggest crucial roles for anti-angiogenic factors, such as endostatin and thrombospondin-1, in assuring proper angiogenesis. Although the exact role of anti-angiogenic factors in recovery from ischemia still needs further clarification, this hypothesis receives strong support from our findings that revascularization is reduced in SorCS2 mutant brains.

Regenerative Therapies GSC 203), by the Berlin Institute of Health (TRG7), and by the German Federal Ministry of Education and Research (BMBF CSB 01EO1301) to C.H., S.M., P.B.S., U.D., by the BMBF under ERA-NET NEURON scheme (01EW1811) to P.B.S., by the Foundation for Polish Science co-financed by the European Union under the European Regional Development Fund (Homing program, POIR.04.04.00 00 5CEF/18 00) to A.R.M., and by the Deutsche Forschungsgemeinschaft under Germany's Excellence Strategy—EXC-2049—390688087. C.J.H. is a participant in the Charité Clinical Scientist Program.

CONFLICT OF INTEREST

The authors declare no conflicts of interest.

DATA AVAILABILITY STATEMENT

The authors confirm that the data supporting the findings of this study are available within the article and its Supporting Information.

ORCID

Anna R. Malik (iD) https://orcid.org/0000-0001-7732-0756

REFERENCES

Aronica, E., Gorter, J. A., Rozemuller, A. J., Yankaya, B., & Troost, D. (2005). Interleukin-1 beta down-regulates the expression of metabotropic glutamate receptor 5 in cultured human astrocytes. *Journal of Neuroimmunology*, 160(1–2), 188–194. https://doi.org/10.1016/j.jneuroim.2004.11.015

Canuel, M., Korkidakis, A., Konnyu, K., & Morales, C. R. (2008). Sortilin mediates the lysosomal targeting of cathepsins D and H. *Biochemical and Biophysical Research Communications*, 373(2), 292–297. https://doi.org/10.1016/j.bbrc.2008.06.021

Chen, J.-Y., Yu, Y., Yuan, Y., Zhang, Y.-J., Fan, X.-P., Yuan, S.-Y., … Yao, S.-L. (2017). Enriched housing promotes post-stroke functional recovery through astrocytic HMGB1-IL-6-mediated angiogenesis. *Cell Death Discovery*, 3, 17054. https://doi.org/10.1038/cddiscovery.2017.54

Chen, N., Gao, R.-F., Yuan, F.-L., & Zhao, M.-D. (2016). Recombinant human endostatin suppresses mouse osteoclast formation by inhibiting the NF-κB and MAPKs signaling pathways. *Frontiers in Pharmacology*, 7, 145. https://doi.org/10.3389/fphar.2016.00145

Chen, Z.-Y., Ieraci, A., Teng, H., Dall, H., Meng, C.-X., Herrera, D. G., … Lee, F. S. (2005). Sortilin controls intracellular sorting of brain-derived neurotrophic factor to the regulated secretory pathway. *The Journal of Neuroscience: The Official Journal of the Society for Neuroscience*, 25(26), 6156–6166. https://doi.org/10.1523/JNEUROSCI.1017-05.2005

Dirnagl, U., & Members of the MCAO-SOP Group. (2012). Standard operating procedures (SOP) in experimental stroke research: SOP for middle cerebral artery occlusion in the mouse. *Nature Precedings*. https://doi.org/10.1038/npre.2012.3492.3

Felbor, U., Dreier, L., Bryant, R. A., Ploegh, H. L., Olsen, B. R., & Mothes, W. (2000). Secreted cathepsin L generates endostatin from collagen XVIII. *The EMBO Journal*, 19(6), 1187–1194. https://doi.org/10.1093/emboj/19.6.1187

Ferreras, M., Felbor, U., Lenhard, T., Olsen, B. R., & Delaissé, J.-M. (2000). Generation and degradation of human endostatin proteins by various proteinases. *FEBS Letters*, 486(3), 247–251. https://doi.org/10.1016/S0014-5793(00)02249-3

Gertz, K., Priller, J., Kronenberg, G., Fink, K. B., Winter, B., Schröck, H., … Endres, M. (2006). Physical activity improves long-term stroke outcome via endothelial nitric oxide synthase-dependent augmentation of neovascularization and cerebral blood flow. *Circulation Research*, 99(10), 1132–1140. https://doi.org/10.1161/01.RES.0000250175.14861.77

Glerup, S., Olsen, D., Vaegter, C. B., Gustafsen, C., Sjoegaard, S. S., Hermey, G., … Nykjaer, A. (2014). SorCS2 regulates dopaminergic wiring and is processed into an apoptotic two-chain receptor in peripheral glia. *Neuron*, 82(5), 1074–1087. https://doi.org/10.1016/j.neuron.2014.04.022

Hayashi, T., Noshita, N., Sugawara, T., & Chan, P. H. (2003). Temporal profile of angiogenesis and expression of related genes in the brain after ischemia. *Journal of Cerebral Blood Flow & Metabolism*, 23(2), 166–180. https://doi.org/10.1097/01.WCB.0000041283.53351.CB

Herda, S., Raczkowski, F., Mittrücker, H.-W., Willimsky, G., Gerlach, K., Kühl, A. A., … Rehm, A. (2012). The sorting receptor Sortilin exhibits a dual function in exocytic trafficking of interferon-γ and granzyme A in T cells. *Immunity*, 37(5), 854–866. https://doi.org/10.1016/j.immuni.2012.07.012

Hou, Q., Ling, L., Wang, F., Xing, S., Pei, Z., & Zeng, J. (2010). Endostatin expression in neurons during the early stage of cerebral ischemia is associated with neuronal apoptotic cell death in adult hypertensive rat model of stroke. *Brain Research*, 1311, 182–188. https://doi.org/10.1016/j.brainres.2009.11.033

Kaplan, R. C., Petersen, A.-K., Chen, M.-H., Teumer, A., Glazer, N. L., Döring, A., … Wallaschofski, H. (2011). A genome-wide association study identifies novel loci associated with circulating IGF-I and IGFBP-3. *Human Molecular Genetics*, 20(6), 1241–1251. https://doi.org/10.1093/hmg/ddq560

Krupinski, J., Kaluza, J., Kumar, P., Kumar, S., & Wang, J. M. (1994). Role of angiogenesis in patients with cerebral ischemic stroke. *Stroke*, 25(9), 1794–1798. https://doi.org/10.1161/01.str.25.9.1794

Kuo, C. J., LaMontagne, K. R., Garcia-Cardeña, G., Ackley, B. D., Kalman, D., Park, S., … Javaherian, K. (2001). Oligomerization-dependent regulation of motility and morphogenesis by the collagen Xviii Nc1/endostatin domain. *The Journal of Cell Biology*, 152(6), 1233–1246. https://doi.org/10.1083/jcb.152.6.1233

Ma, D. H.-K., Yao, J.-Y., Kuo, M.-T., See, L.-C., Lin, K.-Y., Chen, S.-C., … Lin, K.-K. (2007). Generation of endostatin by matrix metalloproteinase and cathepsin from human limbocorneal epithelial cells cultivated on amniotic membrane. *Investigative Ophthalmology & Visual Science*, 48(2), 644–651. https://doi.org/10.1167/iovs.06-0884

Malik, A. R., Szydlowska, K., Nizinska, K., Asaro, A., van Vliet, E. A., Popp, O., … Willnow, T. E. (2019). SorCS2 controls functional expression of amino acid transporter EAAT3 and protects neurons from oxidative stress and epilepsy-induced pathology. *Cell Reports*, 26(10), 2792–2804.e6. https://doi.org/10.1016/j.celrep.2019.02.027

Meng, H., Song, Y., Zhu, J., Liu, Q., Lu, P., Ye, N., … Wu, H. (2016). LRG1 promotes angiogenesis through upregulating the TGF-β1 pathway in ischemic rat brain. *Molecular Medicine Reports*, 14(6), 5535–5543. https://doi.org/10.3892/mmr.2016.5925

Navarro-Sobrino, M., Rosell, A., Hernández-Guillamon, M., Penalba, A., Boada, C., Domingues-Montanari, S., … Montaner, J. (2011). A large screening of angiogenesis biomarkers and their association with neurological outcome after ischemic stroke. *Atherosclerosis*, 216(1), 205–211. https://doi.org/10.1016/j.atherosclerosis.2011.01.030

O'Reilly, M. S., Boehm, T., Shing, Y., Fukai, N., Vasios, G., Lane, W. S., … Folkman, J. (1997). Endostatin: An endogenous inhibitor of angiogenesis and tumor growth. *Cell*, 88(2), 277–285. https://doi.org/10.1016/S0092-8674(00)81848-6

Pardali, E., Goumans, M.-J., & ten Dijke, P. (2010). Signaling by members of the TGF-β family in vascular morphogenesis and disease. *Trends in Cell Biology*, 20(9), 556–567. https://doi.org/10.1016/j.tcb.2010.06.006

Parnis, J., Montana, V., Delgado-Martinez, I., Matyash, V., Parpura, V., Kettenmann, H., … Nolte, C. (2013). Mitochondrial exchanger NCLX plays a major role in the intracellular Ca2+ signaling, gliotransmission,

and proliferation of astrocytes. *Journal of Neuroscience*, *33*(17), 7206–7219. https://doi.org/10.1523/JNEUROSCI.5721-12.2013

Pekny, M., Pekna, M., Messing, A., Steinhäuser, C., Lee, J.-M., Parpura, V., … Verkhratsky, A. (2016). Astrocytes: A central element in neurological diseases. *Acta Neuropathologica*, *131*(3), 323–345. https://doi.org/10.1007/s00401-015-1513-1

Ramakers, C., Ruijter, J. M., Deprez, R. H. L., & Moorman, A. F. M. (2003). Assumption-free analysis of quantitative real-time polymerase chain reaction (PCR) data. *Neuroscience Letters*, *339*(1), 62–66. https://doi.org/10.1016/s0304-3940(02)01423-4

Reitz, C. (2015). The role of the retromer complex in aging-related neurodegeneration: A molecular and genomic review. *Molecular Genetics and Genomics: MGG*, *290*(2), 413–427. https://doi.org/10.1007/s00438-014-0939-9

Ruijter, J. M., Ramakers, C., Hoogaars, W. M. H., Karlen, Y., Bakker, O., van den Hoff, M. J. B., & Moorman, A. F. M. (2009). Amplification efficiency: Linking baseline and bias in the analysis of quantitative PCR data. *Nucleic Acids Research*, *37*(6), e45. https://doi.org/10.1093/nar/gkp045

Rust, R., Grönnert, L., Gantner, C., Enzler, A., Mulders, G., Weber, R. Z., … Schwab, M. E. (2019). Nogo-A targeted therapy promotes vascular repair and functional recovery following stroke. *Proceedings of the National Academy of Sciences of the United States of America*, *116*(28), 14270–14279. https://doi.org/10.1073/pnas.1905309116

Sasaki, T., Fukai, N., Mann, K., Göhring, W., Olsen, B. R., & Timpl, R. (1998). Structure, function and tissue forms of the C-terminal globular domain of collagen XVIII containing the angiogenesis inhibitor endostatin. *The EMBO Journal*, *17*(15), 4249–4256. https://doi.org/10.1093/emboj/17.15.4249

Sudhakar, A., Sugimoto, H., Yang, C., Lively, J., Zeisberg, M., & Kalluri, R. (2003). Human tumstatin and human endostatin exhibit distinct antiangiogenic activities mediated by alpha v beta 3 and alpha 5 beta 1 integrins. *Proceedings of the National Academy of Sciences of the United States of America*, *100*(8), 4766–4771. https://doi.org/10.1073/pnas.0730882100

Tian, H.-L., Chen, H., Cui, Y.-H., Xu, T., & Zhou, L.-F. (2007). Increased protein and mRNA expression of endostatin in the ischemic brain tissue of rabbits after middle cerebral artery occlusion. *Neuroscience Bulletin*, *23*(1), 35–40. https://doi.org/10.1007/s12264-007-0005-2

Vaegter, C. B., Jansen, P., Fjorback, A. W., Glerup, S., Skeldal, S., Kjolby, M., … Nykjaer, A. (2011). Sortilin associates with Trk receptors to enhance anterograde transport and neurotrophin signaling. *Nature Neuroscience*, *14*(1), 54–61. https://doi.org/10.1038/nn.2689

Willnow, T. E., Petersen, C. M., & Nykjaer, A. (2008). VPS10P-domain receptors—Regulators of neuronal viability and function. *Nature Reviews. Neuroscience*, *9*(12), 899–909. https://doi.org/10.1038/nrn2516

Yan, J., Greer, J. M., & McCombe, P. A. (2012). Prolonged elevation of cytokine levels after human acute ischaemic stroke with evidence of individual variability. *Journal of Neuroimmunology*, *246*(1), 78–84. https://doi.org/10.1016/j.jneuroim.2012.02.013

Zhang, C., Zhu, Y., Wang, S., Zachory Wei, Z., Jiang, M. Q., Zhang, Y., … Wei, L. (2018). Temporal gene expression profiles after focal cerebral ischemia in mice. *Aging and Disease*, *9*(2), 249–261. https://doi.org/10.14336/AD.2017.0424

Zhu, H., Gui, Q., Hui, X., Wang, X., Jiang, J., Ding, L., … Chen, H. (2017). TGF-β1/Smad3 signaling pathway suppresses cell apoptosis in cerebral ischemic stroke rats. *Medical Science Monitor*, *23*, 366–376. https://doi.org/10.12659/MSM.899195

SUPPORTING INFORMATION

Additional supporting information may be found online in the Supporting Information section at the end of this article.